Supporting Information

Design of active interlayer space in layered oxysulfide photocatalysts NaM-$TiO_{2.2}S_{1.8}$ (M = lanthanoid) for efficient visible light hydrogen evolution

Yusuke Ishii,[a] Chisato Hanafusa,[a] Hajime Suzuki,*[a,b] Daichi Kato,[a] Osamu Tomita,[a] Akinobu Nakada,[a] Shunsuke Nozawa,[c] Akinori Saeki,[d] Ryu Abe*[a]

[a] Department of Energy and Hydrocarbon Chemistry, Graduate School of Engineering, Kyoto University, Nishikyo-ku, Kyoto 615-8510, Japan
[b] Precursory Research for Embryonic Science and Technology (PRESTO), Japan Science and Technology Agency (JST), 4-1-8 Honcho, Kawaguchi, Saitama 332-0012, Japan
[c] Photon Factory (PF), Institute of Materials Structure Science (IMSS), High Energy Accelerator Research Organization (KEK), Tsukuba, Ibaraki 305-0801, Japan
[d] Department of Applied Chemistry, Graduate School of Engineering, Osaka University,2-1 Yamadaoka, Suita, Osaka 565-0871, Japan

* Corresponding Author: suzuki.hajime.7x@kyoto-u.ac.jp, ryu-abe@scl.kyoto-u.ac.jp

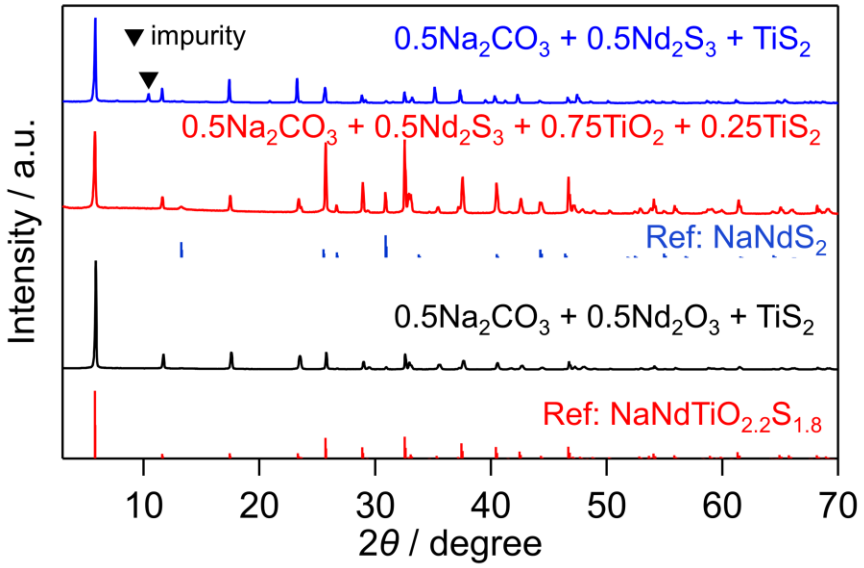

Figure S1. X-ray diffraction (XRD) patterns of the samples obtained *via* solid-state reaction (SSR) using various precursors at 1223 K, along with reference patterns of $NaNdTiO_{2.2}S_{1.8}$ (previous study[1]) and $NaNdS_2$ (ICSD #644913).

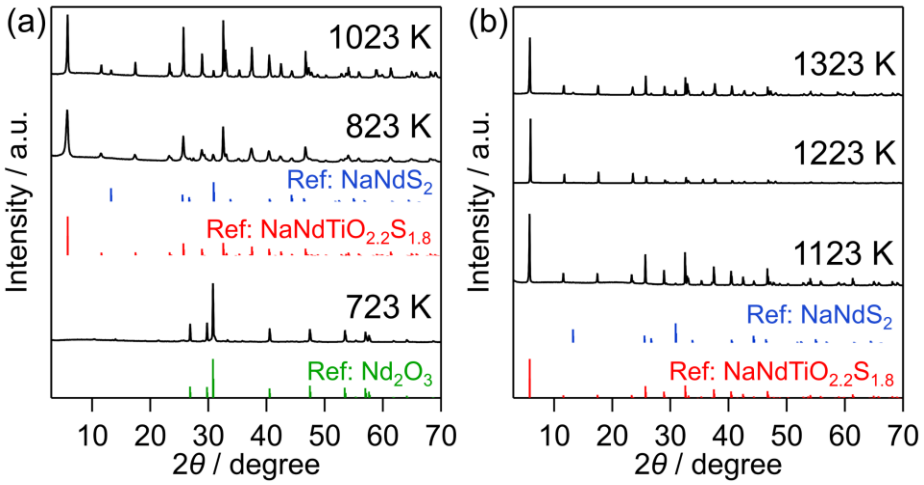

Figure S2. XRD patterns of the samples obtained *via* SSR at various temperatures ((a) 723–1023 K and (b) 1123–1323 K), along with reference patterns of Nd_2O_3 (ICSD #100206), $NaNdTiO_{2.2}S_{1.8}$ (previous study), and $NaNdS_2$ (ICSD #644913).

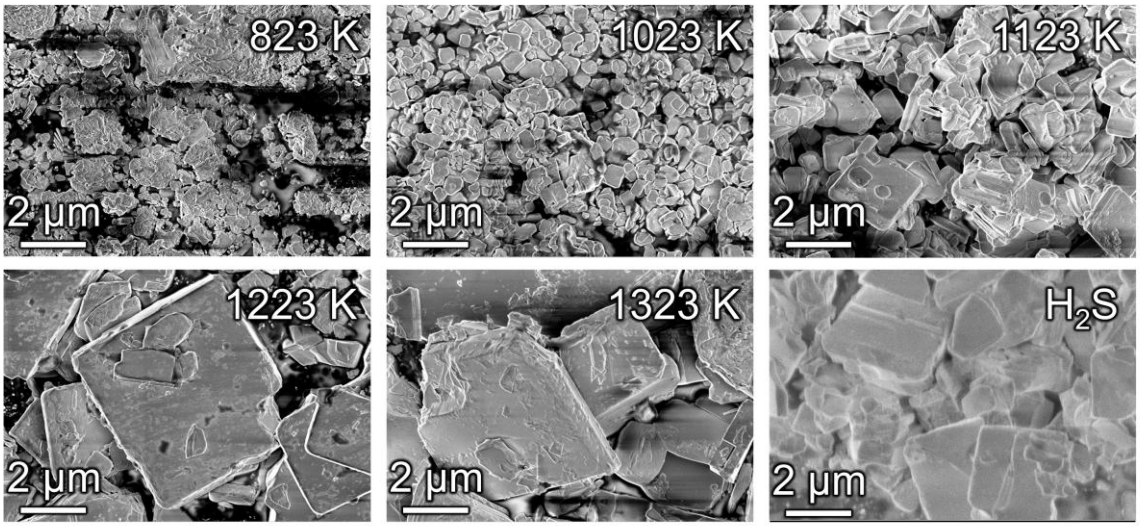

Figure S3. Scanning electron microscopy (SEM) images of $NaNdTiO_{2.2}S_{1.8}$ obtained *via* SSR at 823–1323 K and previous H_2S-based method at 1223 K.

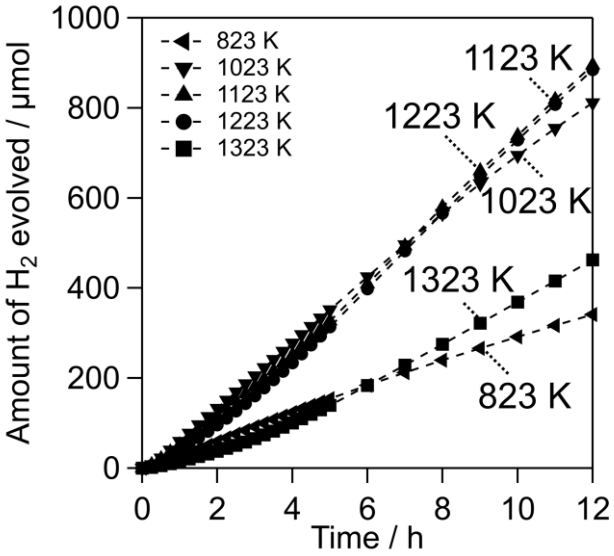

Figure S4. Time courses of photocatalytic H_2 evolution on Rh(out)/$NaNdTiO_{2.2}S_{1.8}$ synthesized *via* SSR at 823–1323 K from water with electron donors (S^{2-} and SO_3^{2-}) under visible light ($400 < \lambda < 800$ nm).

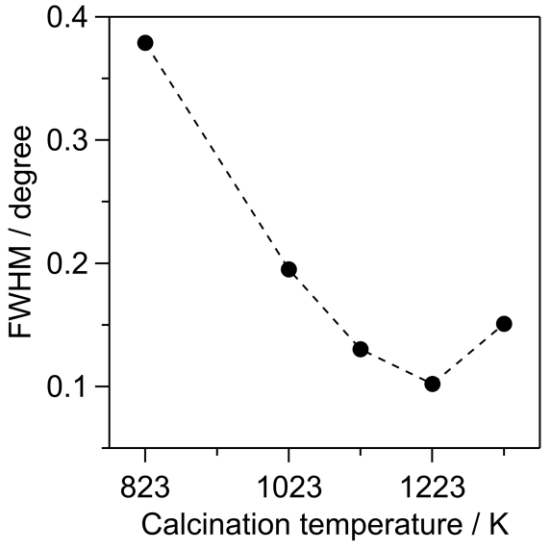

Figure S5. Full width at half maximum (FWHM) of the (001) diffraction peak in the XRD patterns of $NaNdTiO_{2.2}S_{1.8}$ obtained *via* SSR at 823–1323 K.

Table S1. Na/Ti, Nd/Ti, and S/Ti atomic ratios, determined by energy dispersive X-ray spectroscopy (EDX) measurement, for $NaNdTiO_{2.2}S_{1.8}$ obtained *via* SSR at 823–1323 K.

$NaNdTiO_{2.2}S_{1.8}$ (SSR)	Na/Ti	Nd/Ti	S/Ti
823 K	1.11	0.89	1.60
1023 K	1.03	1.03	1.62
1123 K	1.07	1.04	1.59
1223 K	1.13	0.98	1.60
1323 K	0.86	0.95	1.33

The samples synthesized at 1023, 1123, and 1223 K exhibited higher activity than those obtained at the other temperatures. To clarify the origin of this enhanced activity, their crystallinities were compared based on the FWHMs of the XRD pattern and compositional ratios derived from EDX analysis. As shown in Figure S5, the FWHM decreased monotonically from 823 to 1223 K, with a pronounced reduction between 823 and 1023 K. In contrast, the FWHM at 1323 K increased compared to that at 1223 K. Furthermore, the compositional ratios remained nearly constant from 823 to 1223 K (Na/Ti ≈ 1, Nd/Ti ≈ 1, and S/Ti ≈ 1.6), whereas the 1323 K sample exhibited decreased ratios (Na/Ti = 0.86, Nd/Ti = 0.95, and S/Ti = 1.33), indicating the presence of a larger number of Na and S vacancies, likely due to volatilization of Na and S (Table S1). These results demonstrate that the samples synthesized at 1123 and 1223 K possess high crystallinity, leading to their high activities. In contrast, the high activity of the 1023 K sample can be attributed to its moderate crystallinity combined with a smaller particle size.

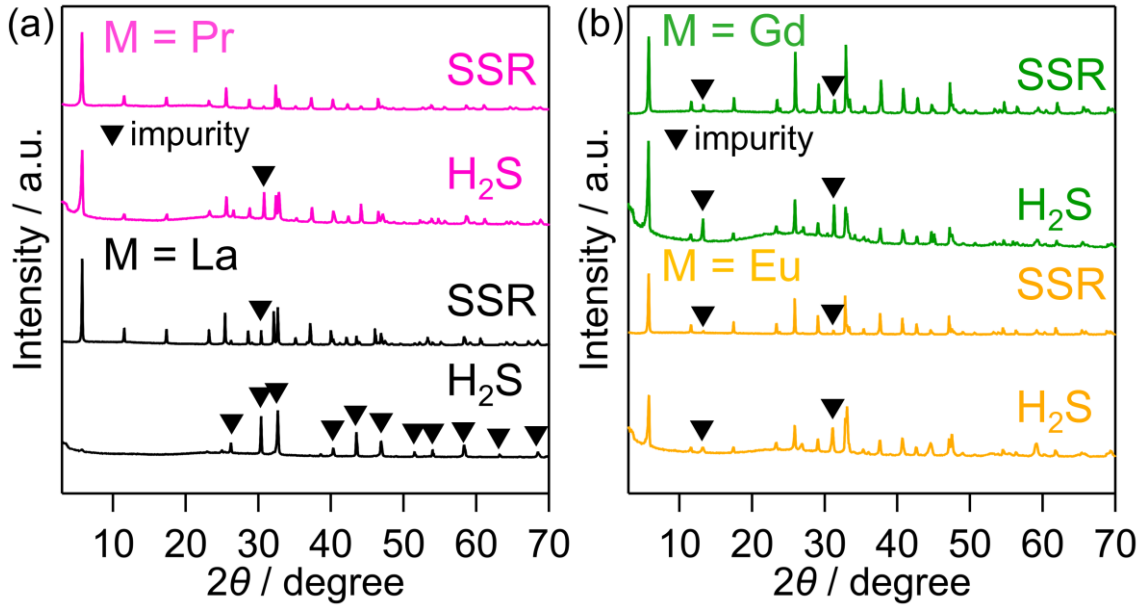

Figure S6. XRD patterns of $NaMTiO_{2.2}S_{1.8}$ (M = La, Pr, Eu, and Gd) obtained *via* SSR at 1023 K and previous H_2S-based method at 1223 K.[1]

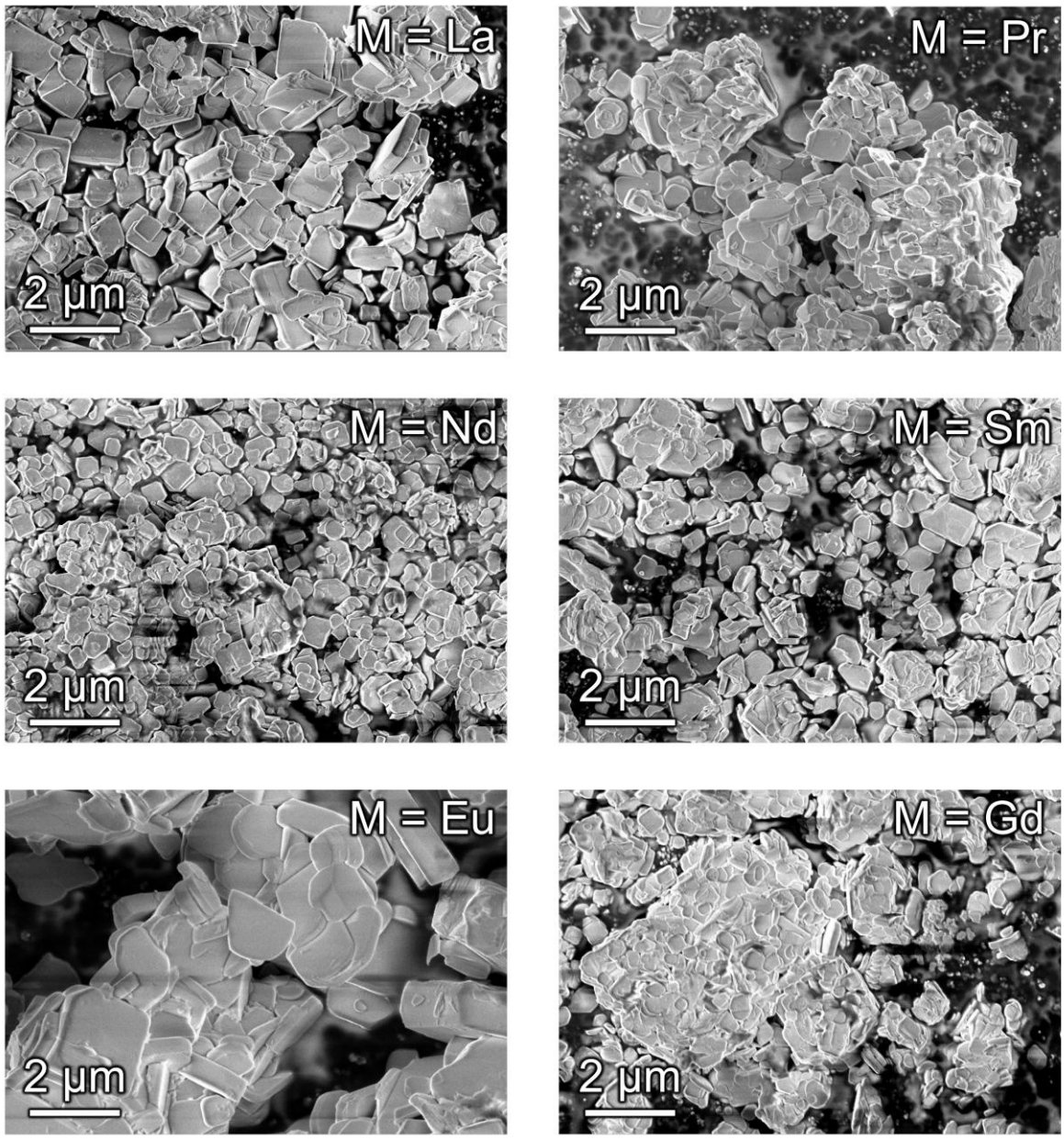

Figure S7. SEM images of $NaMTiO_{2.2}S_{1.8}$ (M = La, Pr, Nd, Sm, Eu, and Gd) obtained *via* SSR at 1023 K.

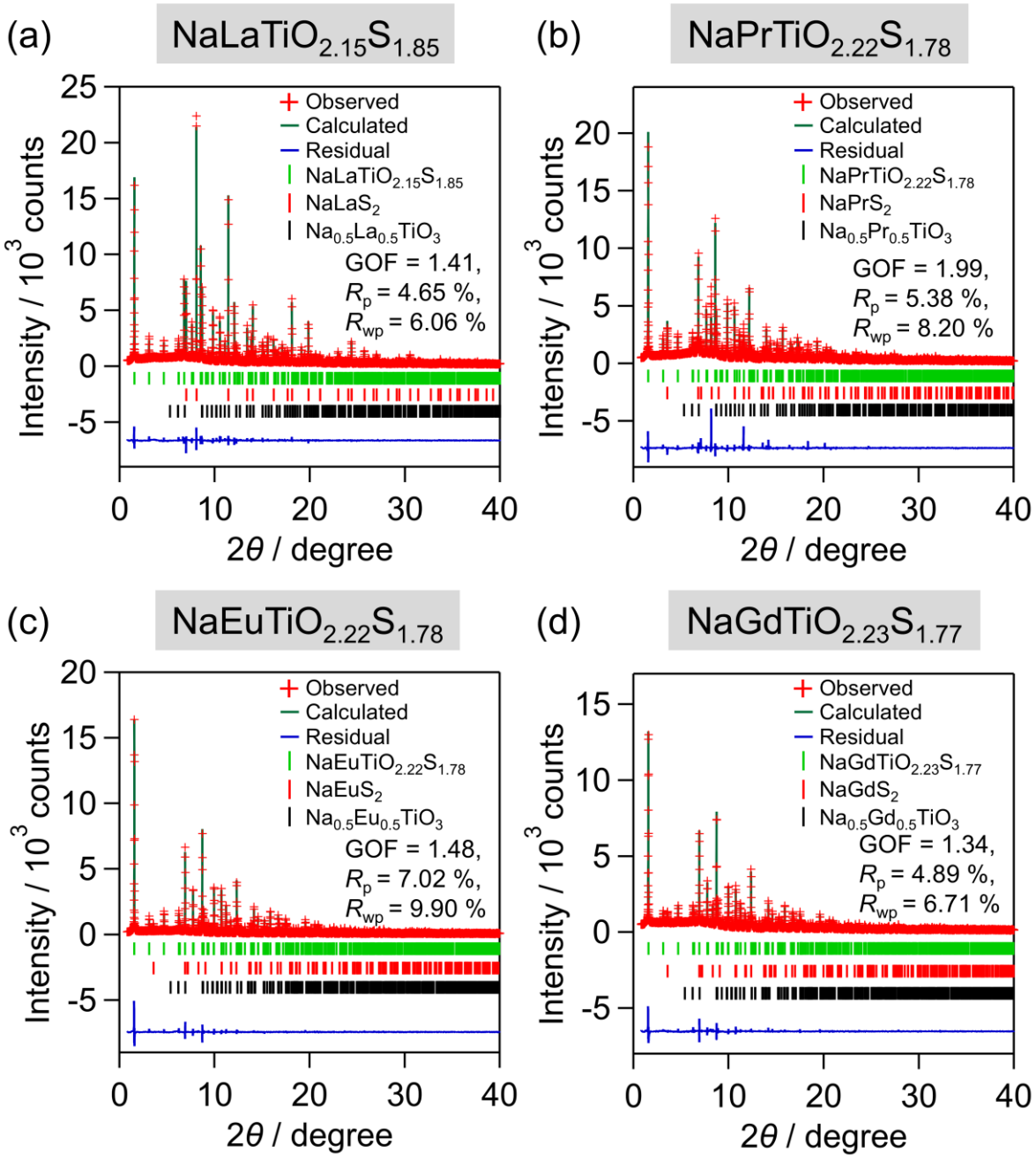

Figure S8. Rietveld refinement of the synchrotron X-ray powder diffraction (SXRPD) patterns of the samples prepared *via* SSR at 1023 K (M = (a) La, (b) Pr, (c) Eu, and (d) Gd) using structural models of $NaMTiO_{2.2}S_{1.8}$ (Figure S9). The red crosses and the green and blue lines represent the observed, calculated, and residual intensities, respectively. Green ticks indicate calculated Bragg reflections of $NaMTiO_{2.2}S_{1.8}$.

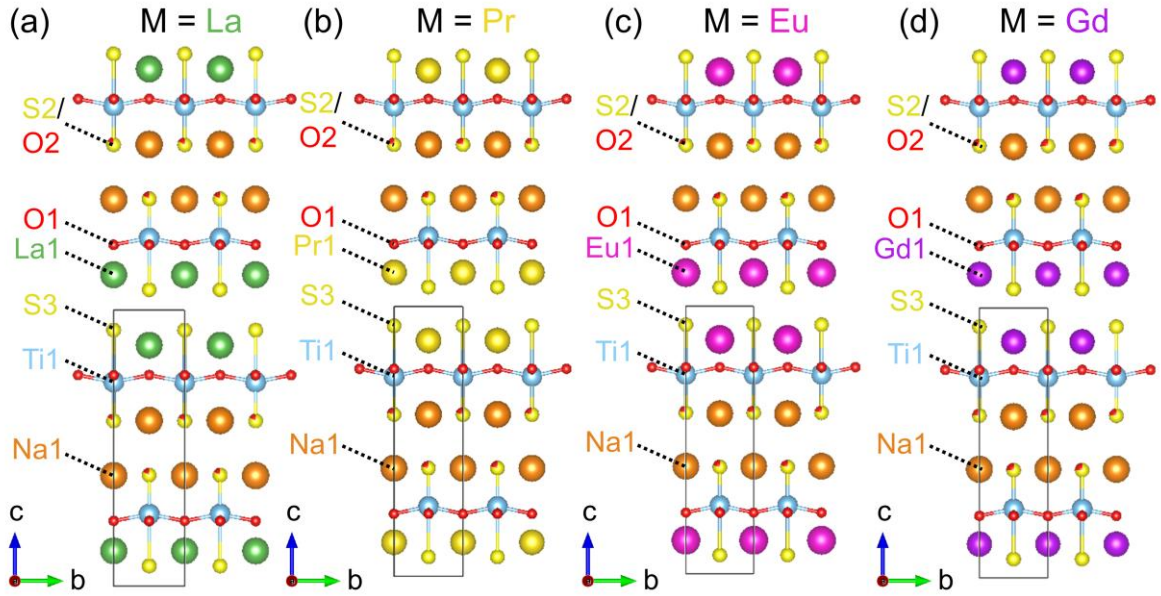

Figure S9. Crystal structures of (a) $NaLaTiO_{2.15}S_{1.85}$, (b) $NaPrTiO_{2.22}S_{1.78}$, (c) $NaEuTiO_{2.22}S_{1.78}$, and (d) $NaGdTiO_{2.23}S_{1.77}$.

Table S2. Refined atomic parameters of $NaLaTiO_{2.15}S_{1.85}$ from the SXRD data of the samples prepared *via* SSR at 1023 K (Figure S8a) using the structural model of $NaLaTiO_{2.15}S_{1.85}$ shown in Figure S9a.

Site	Occupancy	*x*	*y*	*z*	U_{iso} (Å^2)
La1	1	0	0.5	0.8724(3)	0.0069(9)
Na1	1	0	0.5	0.5995(14)	0.034(7)
Ti1	1	0	0.5	0.2605(6)	0.008(2)
O1	1	0	0	0.2360(15)	0.008(5)
S2	0.85(4)	0	0.5	0.4020(9)	0.011(4)
O2	0.15(4)	0	0.5	0.4020(9)	0.011(4)
S3	1	0	0.5	0.0732(9)	0.009(3)

*P*4/*nmm*, $a = b = 3.94042(10)$ Å, $c = 15.3319(7)$ Å, $R_{wp} = 6.06$ %, $R_p = 4.65$ %, GOF = 1.41

Table S3. Refined atomic parameters of $NaPrTiO_{2.22}S_{1.78}$ from the SXRD data of the samples prepared *via* SSR at 1023 K (Figure S8b) using the structural model of $NaPrTiO_{2.22}S_{1.78}$ shown in Figure S9b.

Site	Occupancy	*x*	*y*	*z*	U_{iso} (Å^2)
Pr1	1	0	0.5	0.8739(3)	0.0055(9)
Na1	1	0	0.5	0.5999(16)	0.037(8)
Ti1	1	0	0.5	0.2589(7)	0.007(2)
O1	1	0	0	0.2313(17)	0.007(6)
S2	0.78(5)	0	0.5	0.4007(10)	0.007(5)
O2	0.22(5)	0	0.5	0.4007(10)	0.007(5)
S3	1	0	0.5	0.0718(10)	0.007(3)

*P*4/*nmm*, $a = b = 3.90102(12)$ Å, $c = 15.2626(9)$ Å, $R_{wp} = 8.20$ %, $R_p = 5.38$ %, GOF = 1.99

Table S4. Refined atomic parameters of $NaEuTiO_{2.22}S_{1.78}$ from the SXRD data of the samples prepared *via* SSR at 1023 K (Figure S8c) using the structural model of $NaEuTiO_{2.22}S_{1.78}$ shown in Figure S9c.

Site	Occupancy	*x*	*y*	*z*	U_{iso} (Å^2)
Eu1	1	0	0.5	0.8751(2)	0.0052(8)
Na1	1	0	0.5	0.5982(17)	0.040(8)
Ti1	1	0	0.5	0.2553(7)	0.007(2)
O1	1	0	0	0.2283(15)	0.001(5)
S2	0.78(5)	0	0.5	0.3986(11)	0.012(5)
O2	0.22(5)	0	0.5	0.3986(11)	0.012(5)
S3	1	0	0.5	0.0694(10)	0.007(3)

*P*4/*nmm*, $a = b = 3.85471(7)$ Å, $c = 15.2154(5)$ Å, $R_{wp} = 9.90$ %, $R_p = 7.02$ %, GOF = 1.48

Table S5. Refined atomic parameters of $NaGdTiO_{2.23}S_{1.77}$ from the SXRD data of the samples prepared *via* SSR at 1023 K (Figure S8d) using the structural model of $NaGdTiO_{2.23}S_{1.77}$ shown in Figure S9d.

Site	Occupancy	*x*	*y*	*z*	U_{iso} (Å^2)
Gd1	1	0	0.5	0.8750(2)	0.0050(7)
Na1	1	0	0.5	0.5976(16)	0.042(8)
Ti1	1	0	0.5	0.2553(6)	0.005(2)
O1	1	0	0	0.2297(15)	0.003(5)
S2	0.77(4)	0	0.5	0.3990(10)	0.013(5)
O2	0.23(4)	0	0.5	0.3990(10)	0.013(5)
S3	1	0	0.5	0.0696(9)	0.007(2)

*P*4/*nmm*, $a = b = 3.84397(7)$ Å, $c = 15.1563(6)$ Å, $R_{wp} = 6.71$ %, $R_p = 4.89$ %, GOF = 1.34

Table S6. Na/Ti, M/Ti, and S/Ti atomic ratios, determined by EDX measurement, for $NaMTiO_{2.2}S_{1.8}$ (M = La, Pr, Sm, Nd, Eu, and Gd) obtained *via* SSR at 1023 K.

$NaMTiO_{2.2}S_{1.8}$ (SSR)	Na/Ti	M/Ti	S/Ti
M = La	0.93	1.13	1.60
M = Pr	0.90	0.96	1.57
M = Nd	1.03	1.03	1.62
M = Sm	0.95	1.00	1.65
M = Eu	0.89	1.01	1.67
M = Gd	1.06	1.03	1.65

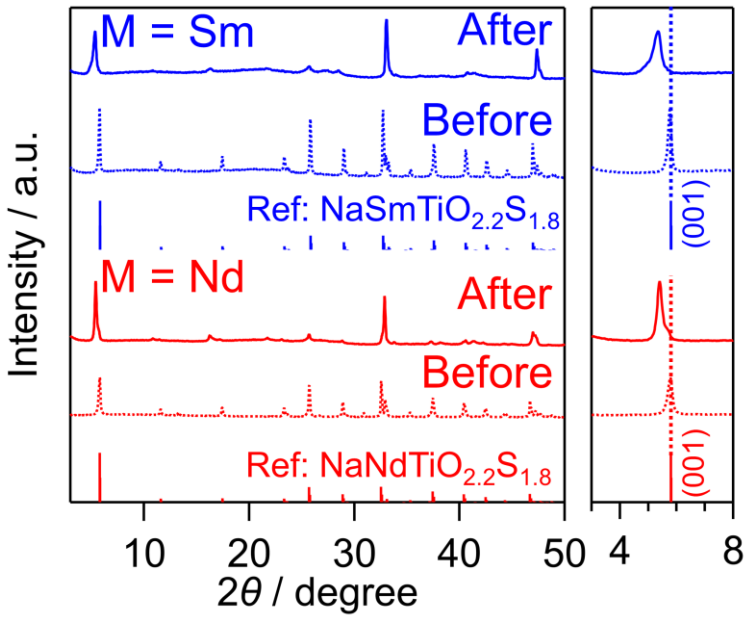

Figure S10. XRD patterns of $NaMTiO_{2.2}S_{1.8}$ (M = Nd and Sm) obtained *via* SSR at 1023 K before and after immersion in a H_2SO_4 aqueous solution (pH = 2.5) for 1 h under dark conditions, along with reference patterns of $NaMTiO_{2.2}S_{1.8}$ (previous study).

Table S7. Na/Ti atomic ratio, determined by EDX measurement, for $NaMTiO_{2.2}S_{1.8}$ (M = La, Pr, Sm, Nd, Eu, and Gd) after immersion in a H_2SO_4 aqueous solution (pH = 2.5) for 1 h under dark conditions.

$NaMTiO_{2.2}S_{1.8}$ (SSR)	Before	After
M = La	0.93	0.5
M = Pr	0.90	0.2
M = Nd	1.03	0.26
M = Sm	0.95	0.11
M = Eu	0.89	0.07
M = Gd	1.06	0.22

Table S8. S/Ti atomic ratio, determined by EDX measurement, for $NaMTiO_{2.2}S_{1.8}$ (M = La, Pr, Sm, Nd, Eu, and Gd) after immersion in a H_2SO_4 aqueous solution (pH = 2.5) for 1 h under dark conditions.

$NaMTiO_{2.2}S_{1.8}$ (SSR)	Before	After
M = Pr	1.57	0.95
M = Nd	1.62	0.95
M = Sm	1.65	0.93
M = Eu	1.67	0.91
M = Gd	1.65	0.93

As previously reported,[1] the S2 site in $NaMTiO_{2.2}S_{1.8}$ is less stable than the S3 site, making O/S substitution more likely to occur. Consequently, after immersion in the H_2SO_4 aqueous solution, all samples exhibited S/Ti ratios close to 1 (Table S8). When approximating the compositions of the H_2SO_4-treated samples as $H_xNa_{1-x}MTiO_{4-y}S_y \cdot nH_2O$, the parameter y was fixed at 1, and this value was also used in the thermogravimetric-differential thermal analysis (TG-DTA) shown in Figure S11.

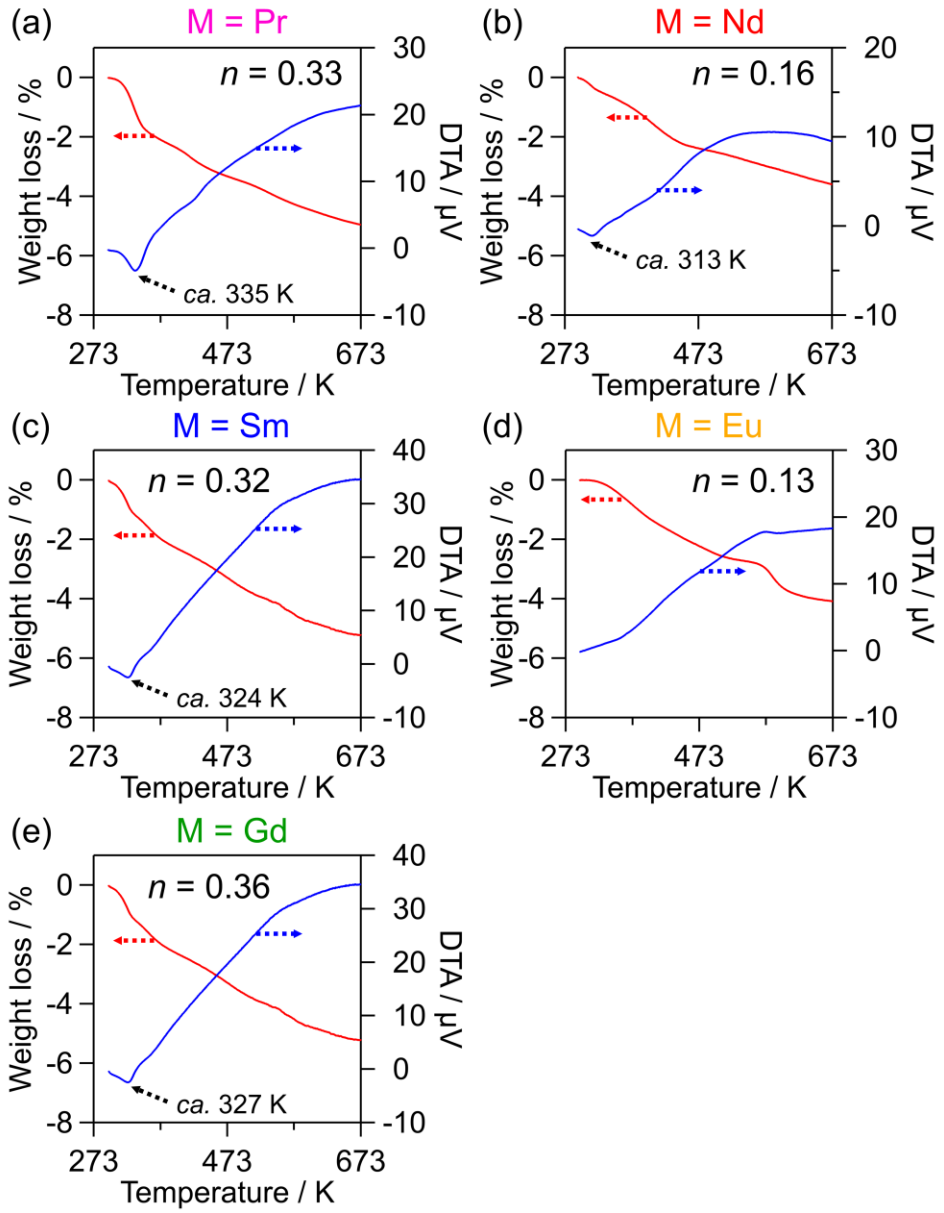

Figure S11. TG-DTA profiles under an N_2 flow (100 mL/min) of $NaMTiO_{2.2}S_{1.8}$ (M = (a) Pr, (b) Nd, (c) Sm, (d) Eu, and (e) Gd) obtained *via* SSR at 1023 K after immersion in a H_2SO_4 aqueous solution (pH = 2.5) for 1 h under dark conditions.

To estimate the amount of interlayer hydration, TG-DTA measurements were performed for $NaMTiO_{2.2}S_{1.8}$ after immersion in a H_2SO_4 aqueous solution (pH = 2.5) for 1 h. For all samples except M = Eu, negative DTA peaks (endothermic peaks) were observed at 313–335 K, which are attributable to the release of interlayer water molecules. The dehydration in this temperature range has also been reported for similar layered oxides such as $NaNdTiO_4$.[2] Therefore, we assume that the mass loss up to 373 K, at which this peak disappeared, corresponds to the removal of interlayer water. The obtained composition was approximated as $H_xNa_{1-x}MTiO_{4-y}S_y \cdot nH_2O$, where x was determined by EDX analysis (Table S7), and y was fixed at 1 (Table S8). Based on these assumptions, the interlayer hydration amount n was estimated.

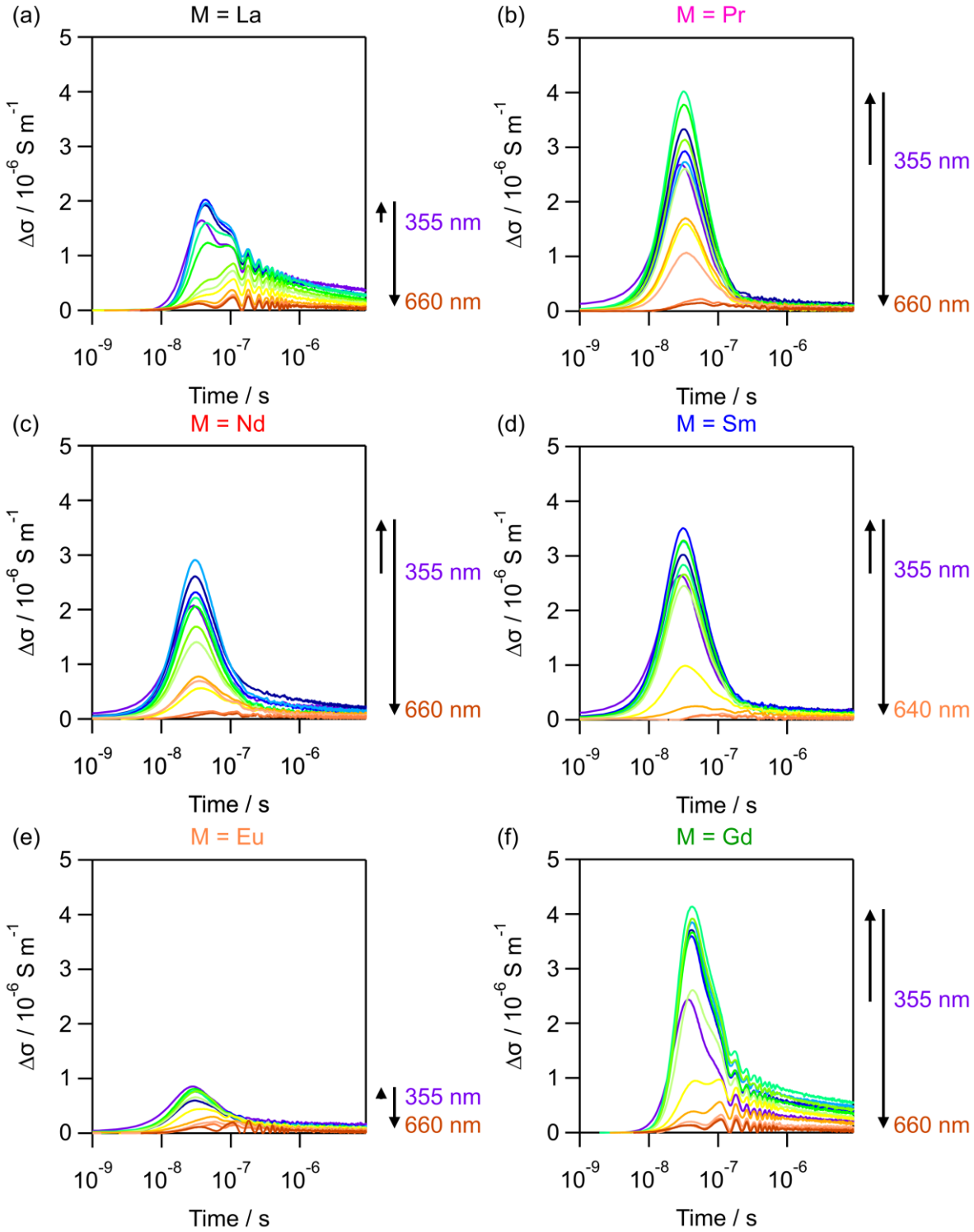

Figure S12. Photoconductivity transients ($\Delta\sigma$) obtained by time-resolved microwave conductivity (TRMC) measurements for $NaMTiO_{2.2}S_{1.8}$ (M = (a) La, (b) Pr, (c) Nd, (d) Sm, (e) Eu, and (f) Gd) prepared *via* SSR at 1023 K (λ_{ex} = 355–660 nm, $I_0 = 4.6\times10^{15}$ photons cm^{-2} per $pulse^{-1}$).

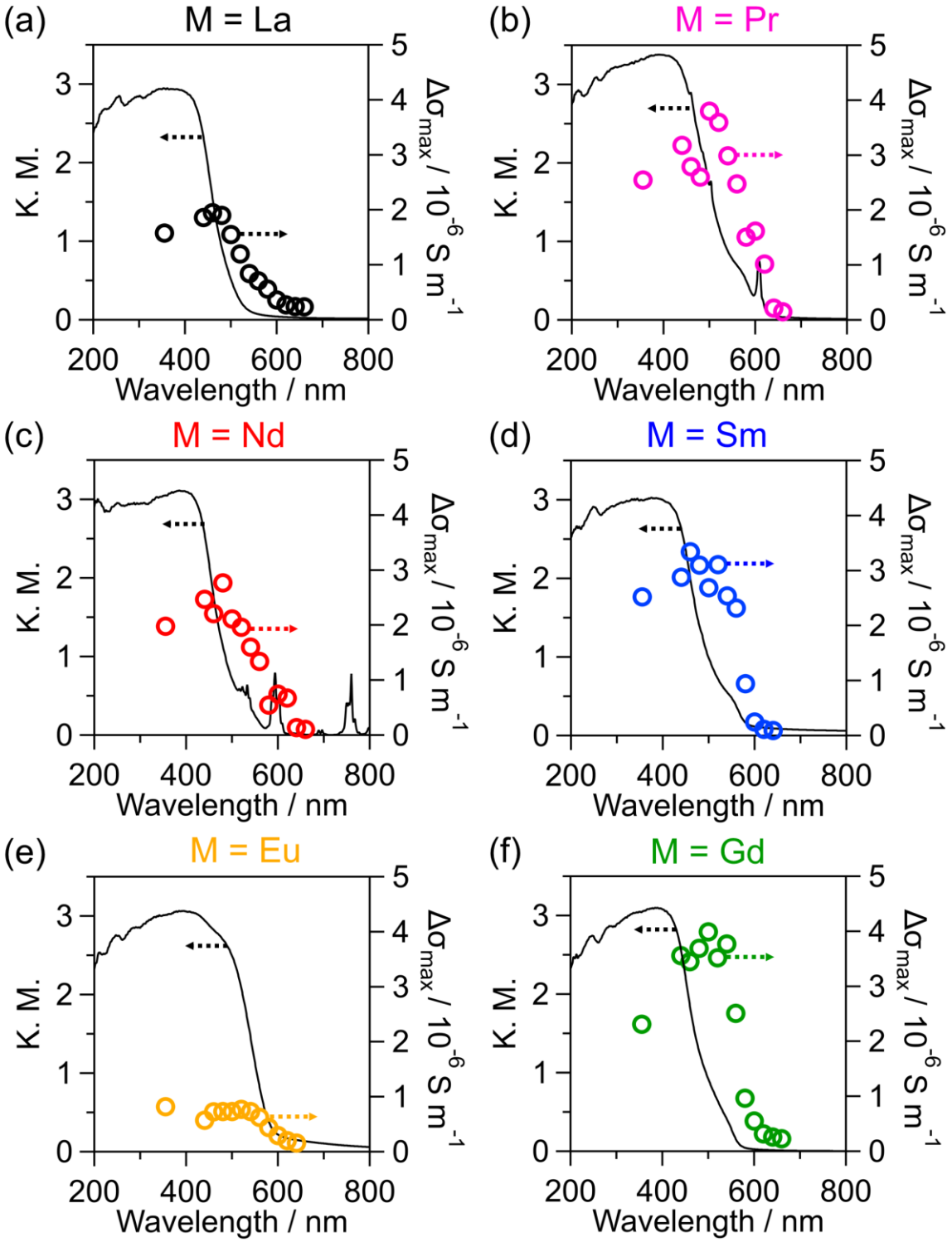

Figure S13. UV-vis diffuse reflectance spectra and wavelength dependence of $\Delta\sigma_{max}$ obtained by TRMC measurements of $NaMTiO_{2.2}S_{1.8}$ (M = (a) La, (b) Pr, (c) Nd, (d) Sm, (e) Eu, and (f) Gd) synthesized *via* SSR at 1023 K.

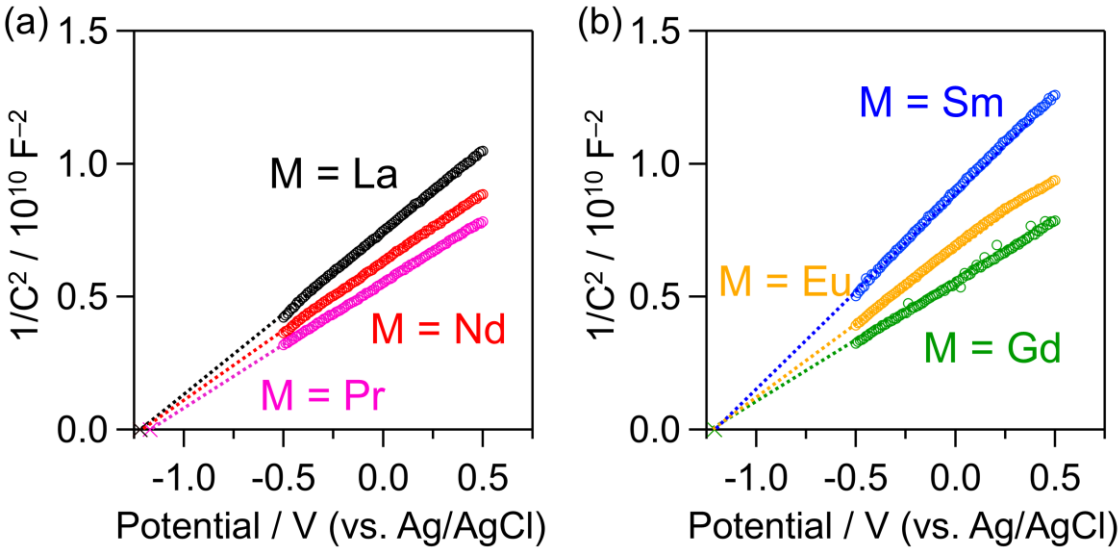

Figure S14. Mott-Schottky plots for $NaMTiO_{2.2}S_{1.8}$ (M = (a) La, Pr, Nd and (b) Sm, Eu, Gd) obtained *via* SSR at 1023 K.

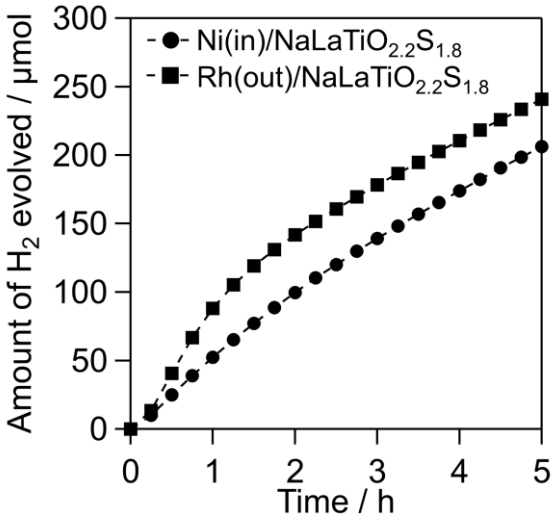

Figure S15. Time courses of photocatalytic H_2 evolution on $Ni(in)/NaLaTiO_{2.2}S_{1.8}$ and $Rh(out)/NaLaTiO_{2.2}S_{1.8}$ from water with electron donors (S^{2-} and SO_3^{2-}) under visible light ($400 < \lambda < 800$ nm).

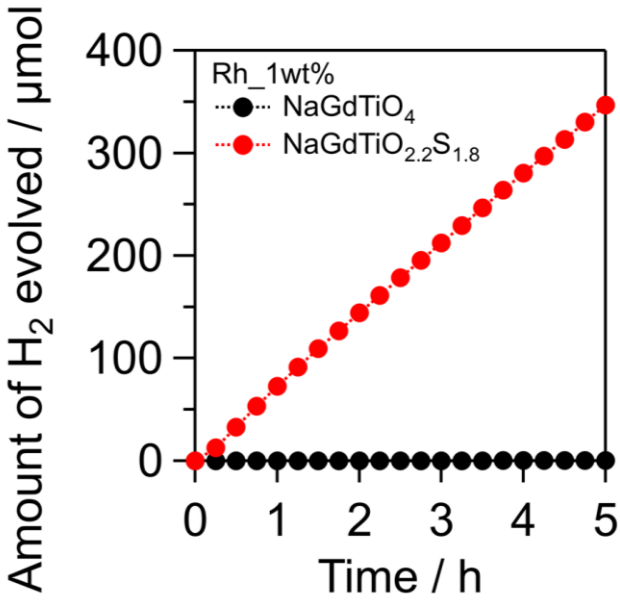

Figure S16. Time courses of photocatalytic H_2 evolution on Rh(out)/$NaGdTiO_4$ and Rh(out)/$NaGdTiO_{2.2}S_{1.8}$ from water with electron donors (S^{2-} and SO_3^{2-}) under visible light ($400 < \lambda < 800$ nm).

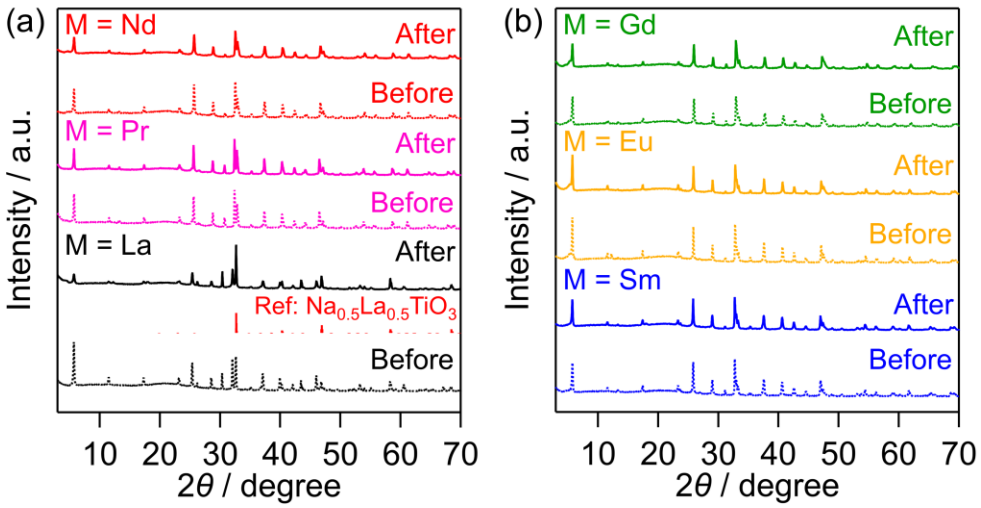

Figure S17. XRD patterns of Ni(in)/$NaMTiO_{2.2}S_{1.8}$ (M = (a) La, Pr, Nd, and (b) Sm, Eu, Gd) before and after the photocatalytic H_2 evolution reaction, along with reference patterns of $Na_{0.5}La_{0.5}TiO_3$ (ICSD #51029).

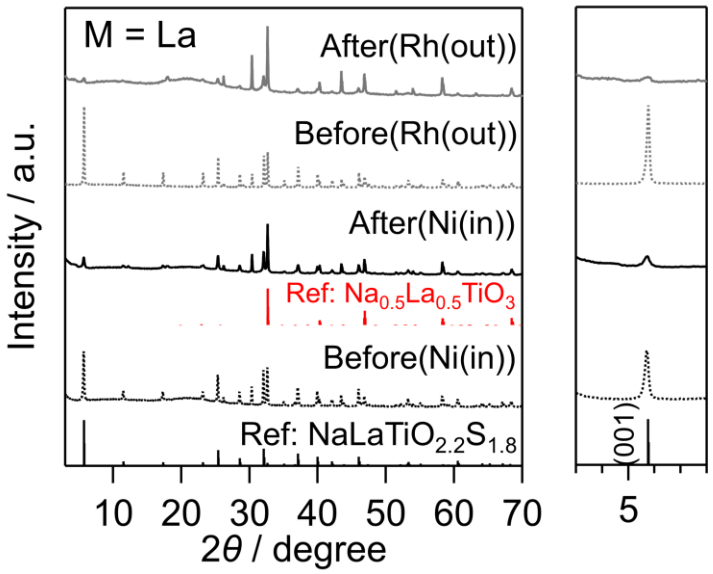

Figure S18. XRD patterns of $NaLaTiO_{2.2}S_{1.8}$ before and after the photocatalytic H_2 evolution reaction (loaded with Ni(in) or Rh(out)), along with reference patterns of $NaLaTiO_{2.2}S_{1.8}$ (this study) and $Na_{0.5}La_{0.5}TiO_3$ (ICSD #51029).

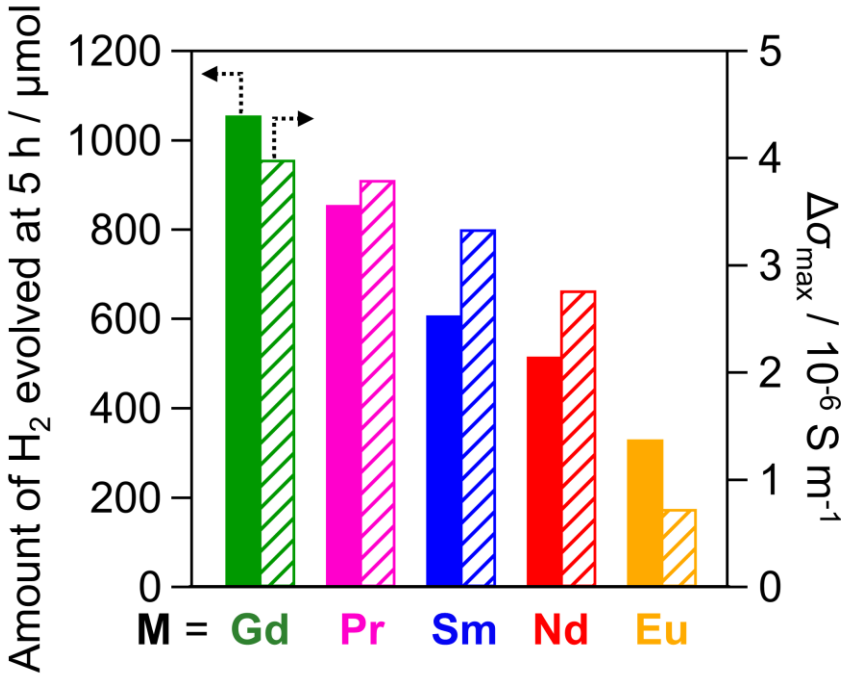

Figure S19. Amount of H_2 evolution at 5 h on Ni(in)/$NaMTiO_{2.2}S_{1.8}$ (M = Pr, Nd, Sm, Eu, and Gd) (solid bars) and $\Delta\sigma_{max}$ obtained from TRMC measurements (λ_{ex} = 460 (M = Sm) or 480 (M = Nd) or 500 nm (M = Pr, Eu, Gd), $I_0 = 4.6 \times 10^{15}$ photons cm^{-2} $pulse^{-1}$) for $NaMTiO_{2.2}S_{1.8}$.

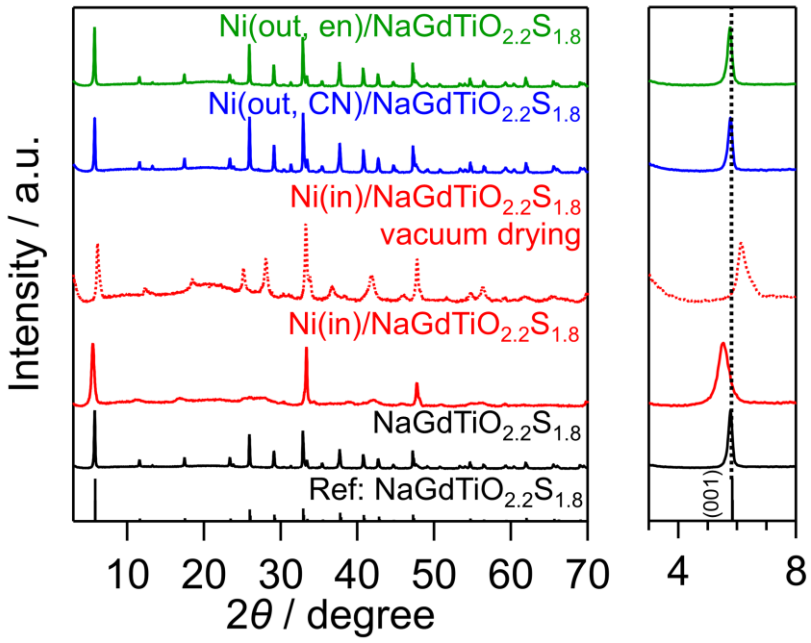

Figure S20. XRD patterns of $NaGdTiO_{2.2}S_{1.8}$ before and after immersion in an $Ni(NO_3)_2$ (Ni(in)), $[Ni(en)_3](NO_3)_2$ (Ni(out, en)) (en = ethylenediamine), or $K_2[Ni(CN)_4]$ (Ni(out, CN)) aqueous solution for 24 h, followed by vacuum drying, along with reference patterns of $NaGdTiO_{2.2}S_{1.8}$ (this study). All treatments were performed using Ni precursor amounts corresponding to a Na:Ni molar ratio of 2:1.

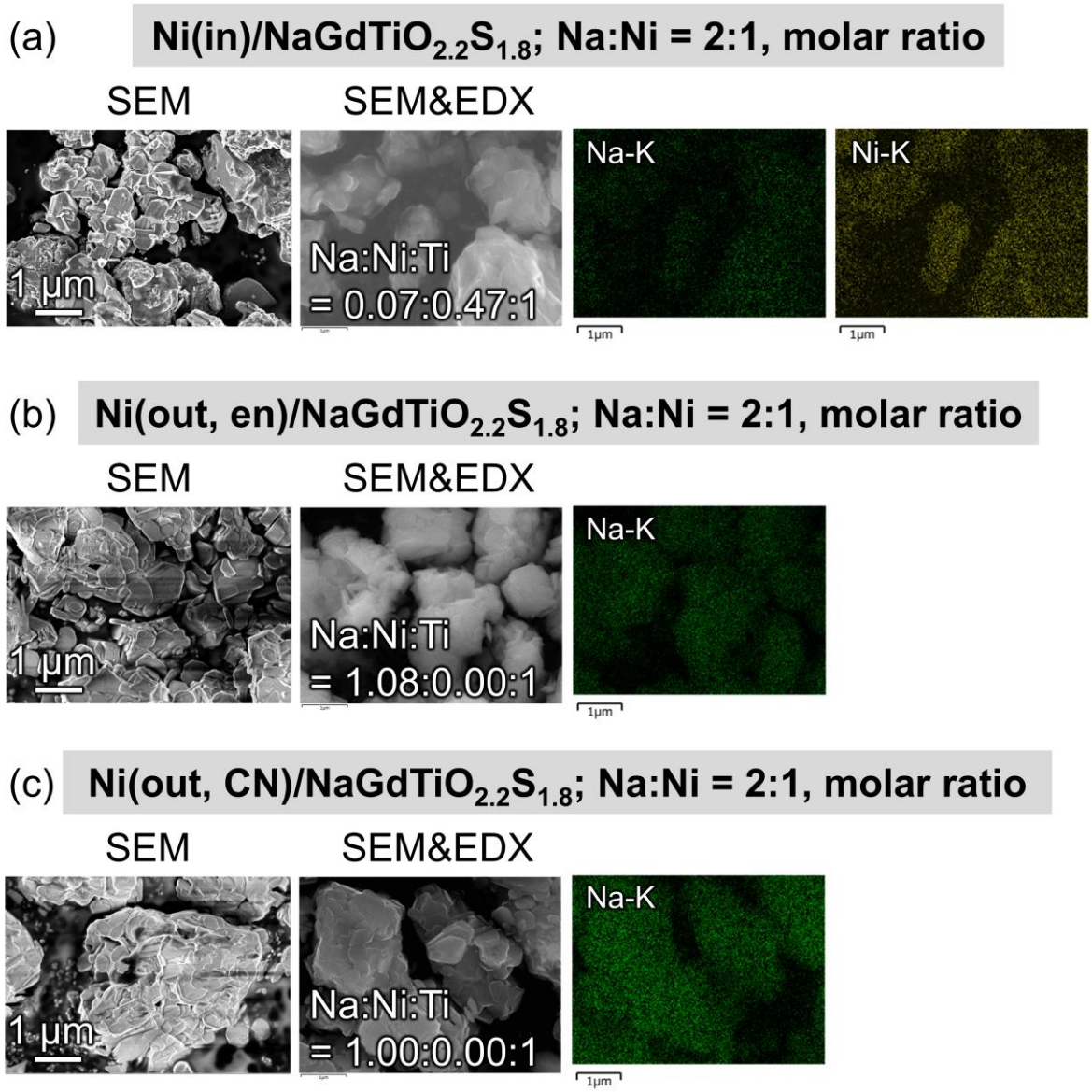

Figure S21. SEM images and SEM-EDX elemental mappings of $NaGdTiO_{2.2}S_{1.8}$ after immersion in an (a) $Ni(NO_3)_2$, (b) $[Ni(en)_3](NO_3)_2$ and (c) $K_2[Ni(CN)_4]$ aqueous solution for 24 h ((a) Ni(in)/$NaGdTiO_{2.2}S_{1.8}$, (b) Ni(out, en)/$NaGdTiO_{2.2}S_{1.8}$ and (c) Ni(out, CN)/$NaGdTiO_{2.2}S_{1.8}$; Na:Ni = 2:1, molar ratio).

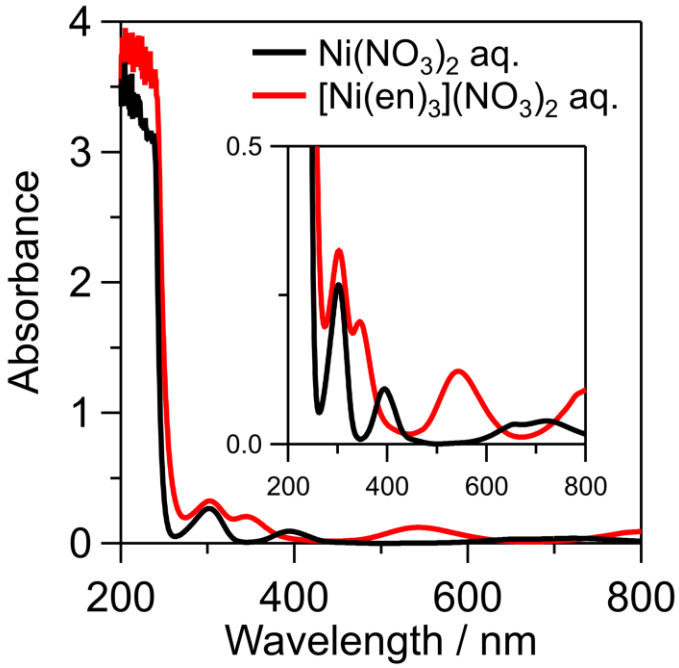

Figure S22. Absorption spectra of $Ni(NO_3)_2$ (black) and $[Ni(en_3)](NO_3)_2$ (red) aqueous solutions used for Ni loading onto $NaMTiO_{2.2}S_{1.8}$.
The absorption spectrum of $[Ni(en)_3]^{2+}$ is consistent with the previously reported spectrum of $[Ni(en)_3]^{2+}$.[3]

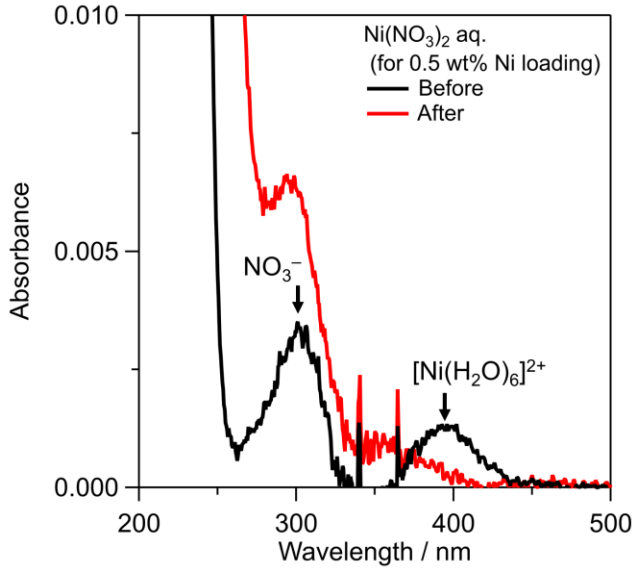

Figure S23. Absorption spectra of aqueous solutions of $Ni(NO_3)_2$ corresponding to a Ni loading amount of 0.5 wt% on $NaGdTiO_{2.2}S_{1.8}$, before and after immersion of $NaGdTiO_{2.2}S_{1.8}$ for 24 h.

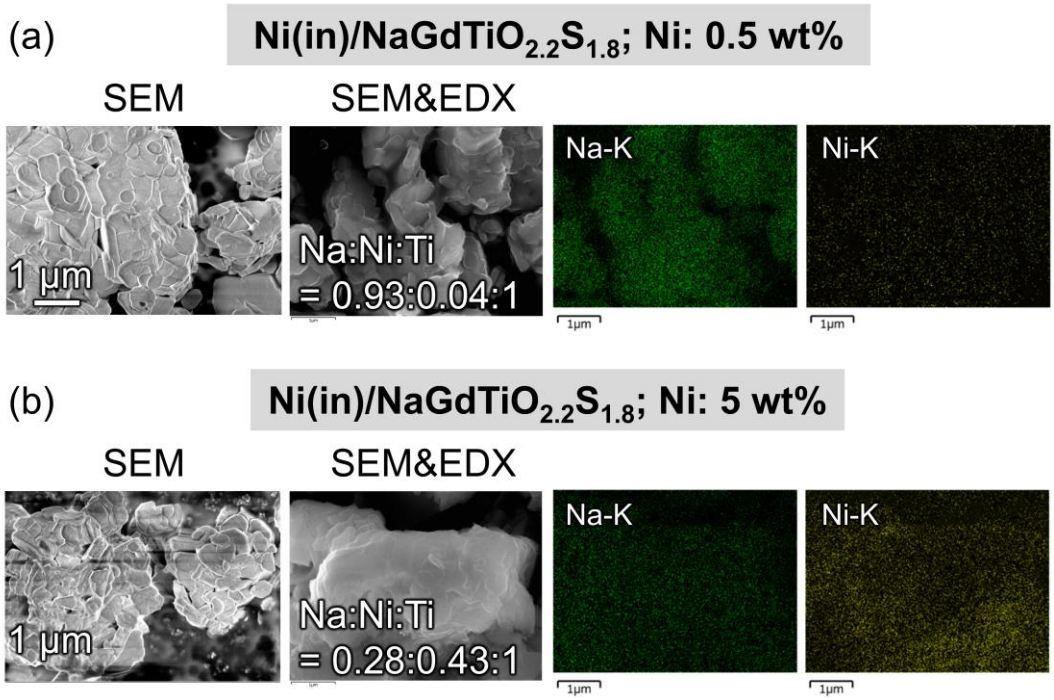

Figure S24. SEM images and SEM-EDX elemental mappings of $NaGdTiO_{2.2}S_{1.8}$ after immersion in an $Ni(NO_3)_2$ aqueous solution for 24 h ($Ni(in)/NaGdTiO_{2.2}S_{1.8}$; Ni: (a) 0.5 and (b) 5 wt% as Ni metal).

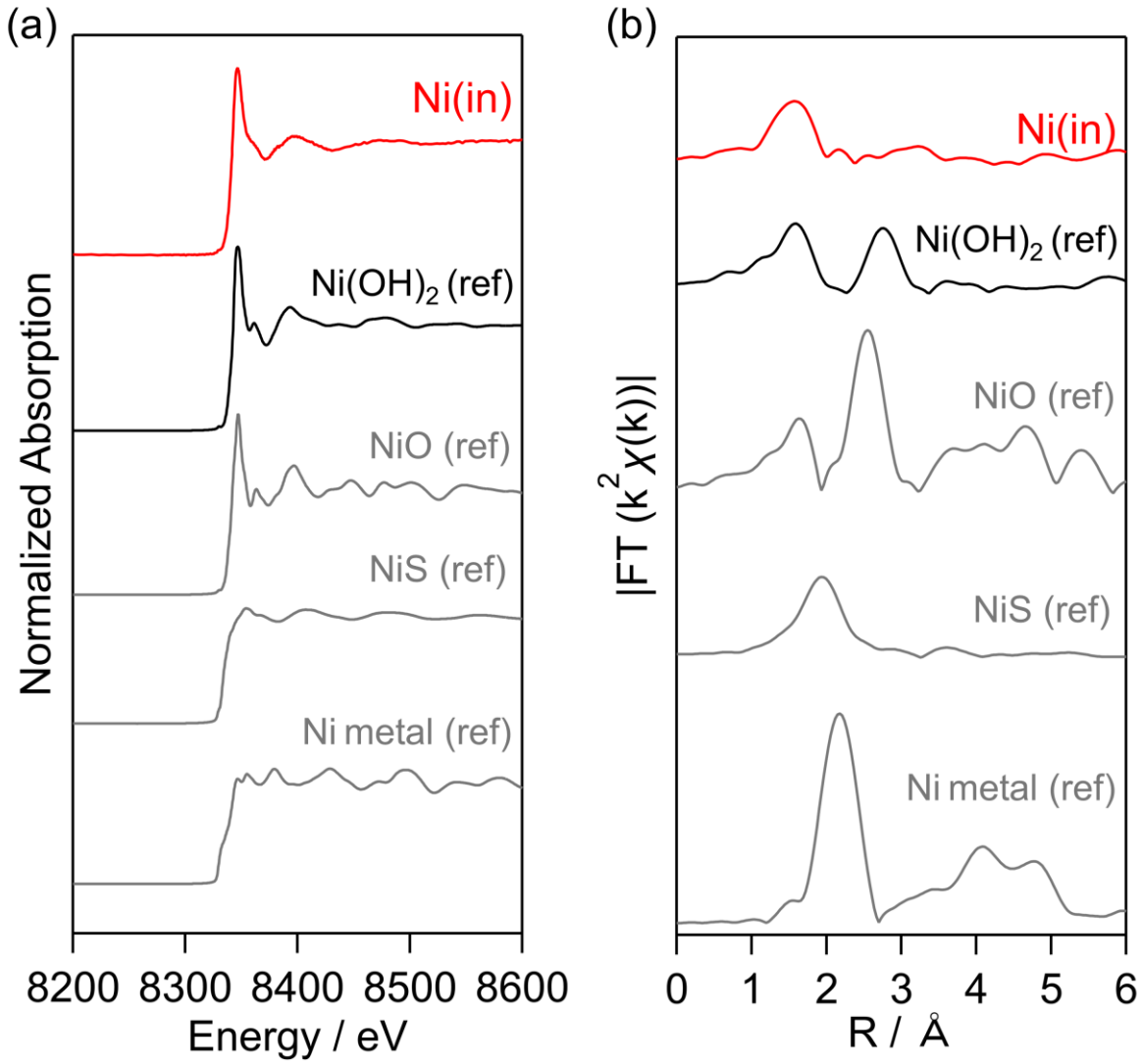

Figure S25. Ni K-edge (a) X-ray absorption near edge structure (XANES) and (b) Fourier transforms of extended X-ray absorption fine structure (EXAFS) spectra of Ni(in)/$NaGdTiO_{2.2}S_{1.8}$ (Ni 0.5 wt% as Ni metal), along with the spectra of reference samples.

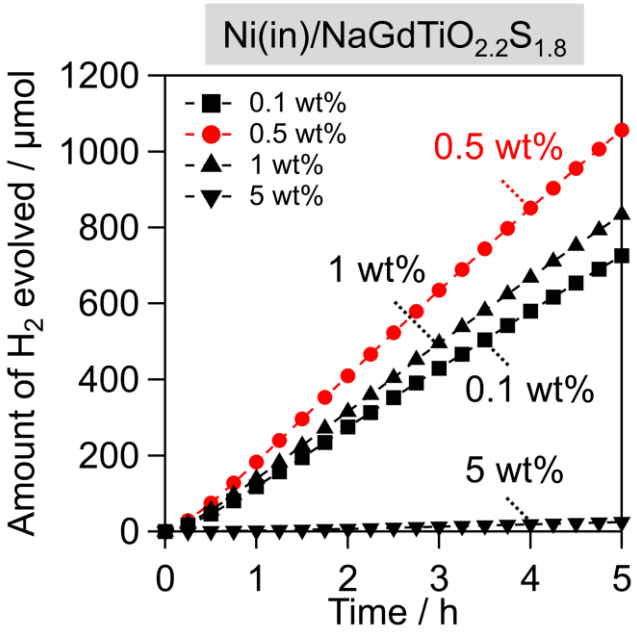

Figure S26. Time courses of photocatalytic H_2 evolution on Ni(in)/$NaGdTiO_{2.2}S_{1.8}$ loaded with different amounts of Ni species from water with electron donors (S^{2-} and SO_3^{2-}) under visible light ($400 < \lambda < 800$ nm).

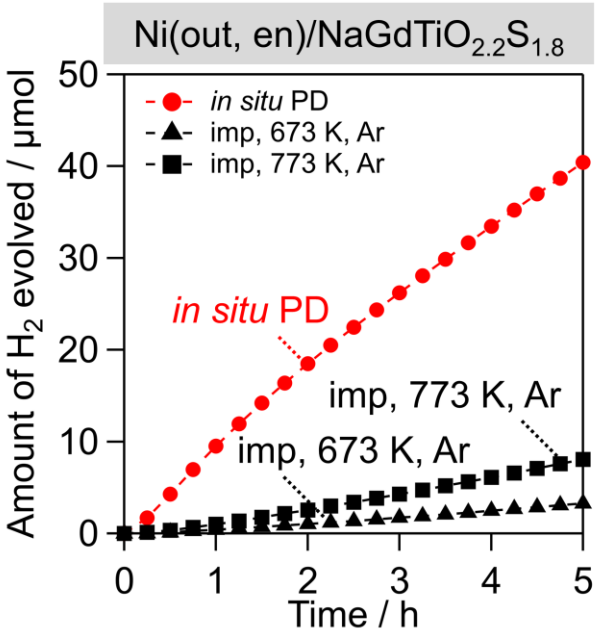

Figure S27. Time courses of photocatalytic H_2 evolution from water with electron donors (S^{2-} and SO_3^{2-}) under visible light ($400 < \lambda < 800$ nm) on Ni(out, en)/$NaGdTiO_{2.2}S_{1.8}$ prepared by *in situ* photodeposition (PD) and by impregnation (imp) and calcination at 673 or 773 K under an Ar flow (20 mL/min), using $[Ni(en)_3](NO_3)_2$ as the Ni precursor (0.5 wt% as Ni metal).

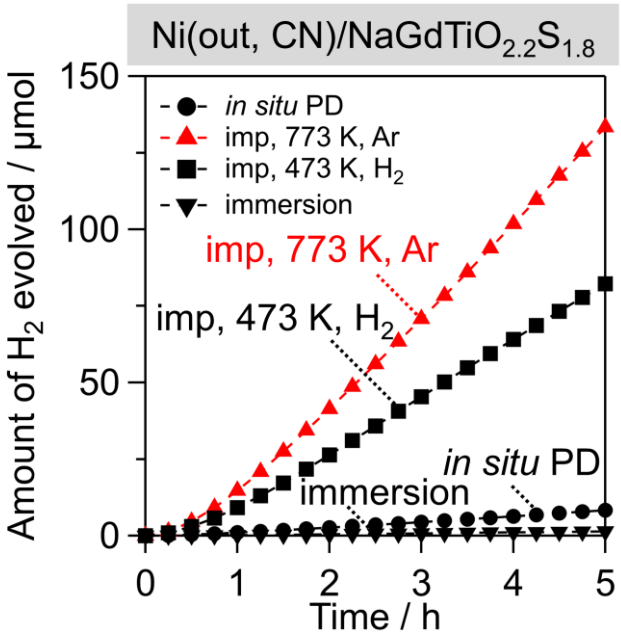

Figure S28. Time courses of photocatalytic H_2 evolution from water with electron donors (S^{2-} and SO_3^{2-}) under visible light ($400 < \lambda < 800$ nm) on Ni(out, CN)/$NaGdTiO_{2.2}S_{1.8}$ prepared by *in situ* PD, by immersion in the Ni precursor aqueous solution for 24 h (immersion) and by impregnation (imp) followed by calcination at 773 K under an Ar flow (20 mL/min) and at 473 K under an H_2 flow (20 mL/min), using $K_2[Ni(CN)_4]$ as the Ni precursor (0.5 wt% as Ni metal).

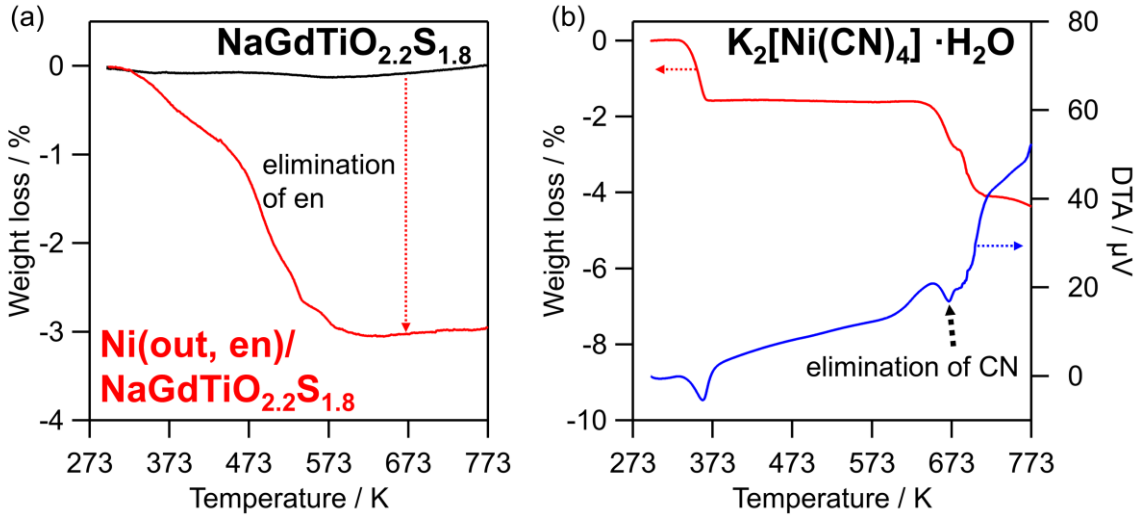

Figure S29. TG-DTA profiles under an N_2 flow (100 mL/min) of (a) $NaGdTiO_{2.2}S_{1.8}$ and Ni(out, en)/$NaGdTiO_{2.2}S_{1.8}$ prepared by the impregnation method before calcination and (b) the Ni precursor $K_2[Ni(CN)_4]\cdot H_2O$ used for surface loading on $NaGdTiO_{2.2}S_{1.8}$.

The calcination temperatures for Ni(out, en)/$NaGdTiO_{2.2}S_{1.8}$ and Ni(out, CN)/$NaGdTiO_{2.2}S_{1.8}$ after impregnation were set above 673 and 773 K, respectively, based on the TG-DTA measurements (Figure S29), at which the dissociation of the en and CN ligands was observed.

Table S9. Amount of photocatalytic H_2 evolution at 5 h on bare $NaGdTiO_{2.2}S_{1.8}$ and 0.5 wt% Ni-loaded $NaGdTiO_{2.2}S_{1.8}$ (Ni(in), Ni(out, CN) and Ni(out, en)), prepared under optimized conditions, from water with electron donors (S^{2-} and SO_3^{2-}) under visible light ($400 < \lambda < 800$ nm).

M/$NaGdTiO_{2.2}S_{1.8}$	M = bare	M = Ni(in)	M = Ni(out, CN)	M = Ni(out, en)
Amount of H_2 evolution at 5 h (μmol)	8.0	1056.7	133.3	40.4

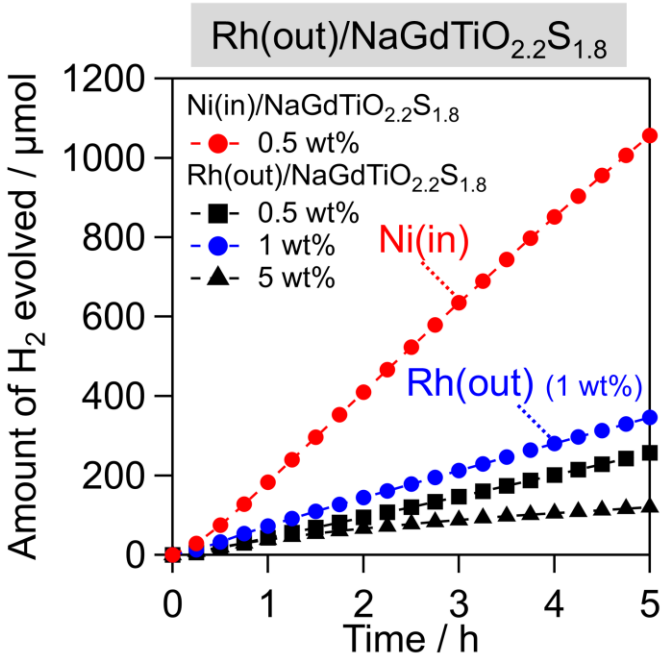

Figure S30. Time courses of photocatalytic H_2 evolution on Ni(in)/$NaGdTiO_{2.2}S_{1.8}$ loaded with 0.5 wt% Ni species (as Ni metal) and Rh(out)/$NaGdTiO_{2.2}S_{1.8}$ loaded with different amounts of Rh species from water with electron donors (S^{2-} and SO_3^{2-}) under visible light ($400 < \lambda < 800$ nm).

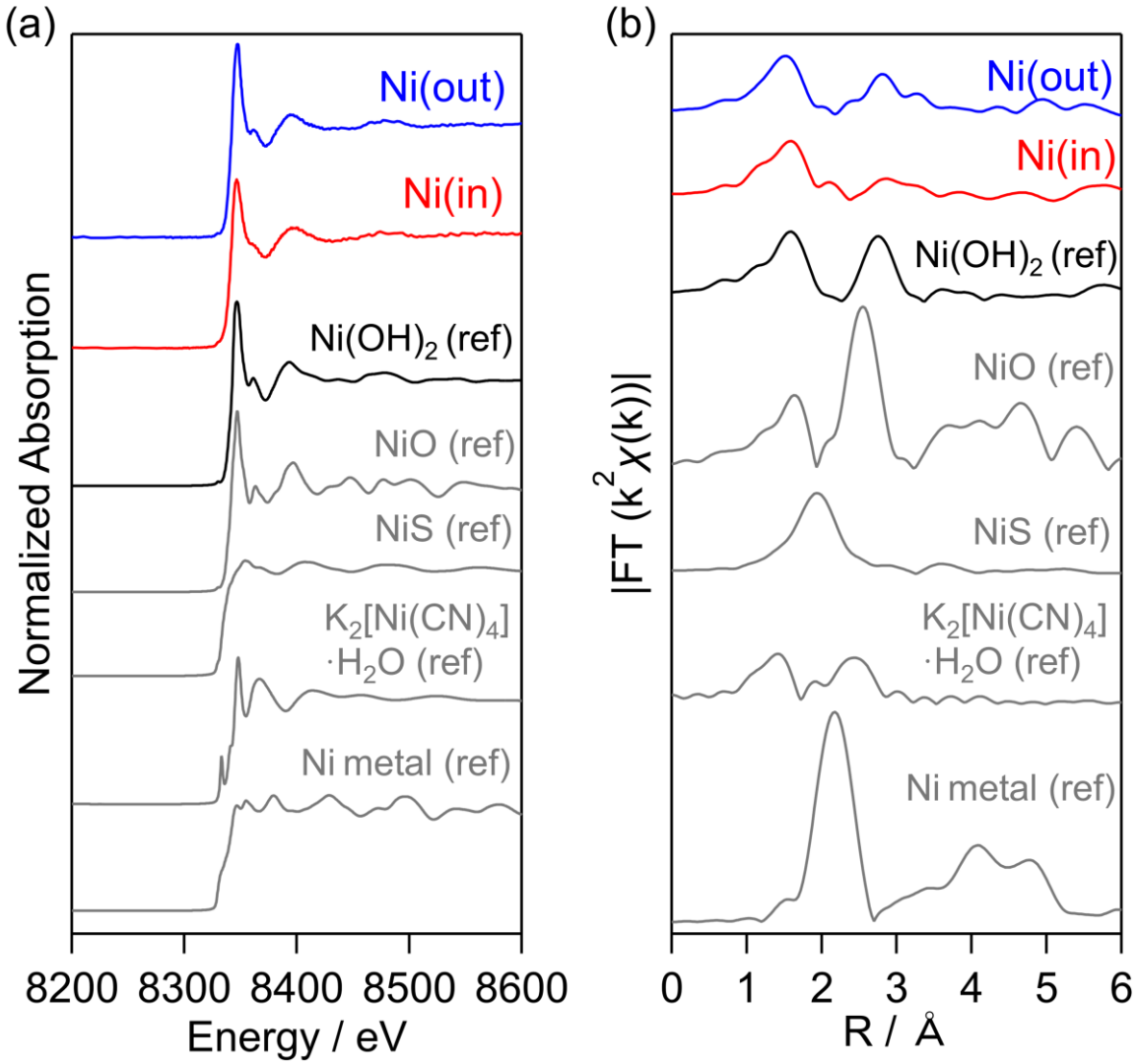

Figure S31. Ni K-edge (a) XANES and (b) Fourier transforms of EXAFS spectra for Ni/$NaGdTiO_{2.2}S_{1.8}$ (Ni(in) and Ni(out)) after the photocatalytic H_2 evolution reaction, along with the spectra of reference samples.

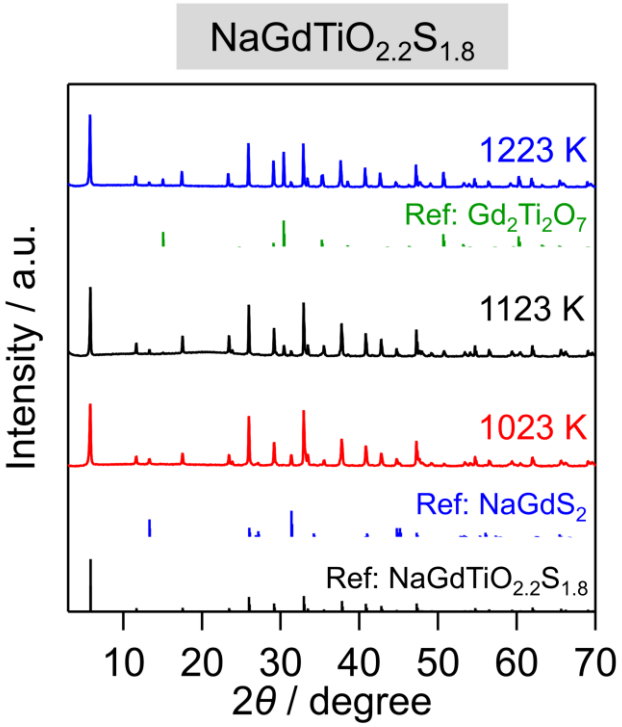

Figure S32. XRD patterns of $NaGdTiO_{2.2}S_{1.8}$ synthesized *via* SSR at 1023–1223 K, along with reference patterns of $NaGdTiO_{2.2}S_{1.8}$ (this study), $NaGdS_2$ (ICSD #48243) and $Gd_2Ti_2O_7$ (ICSD #19687).

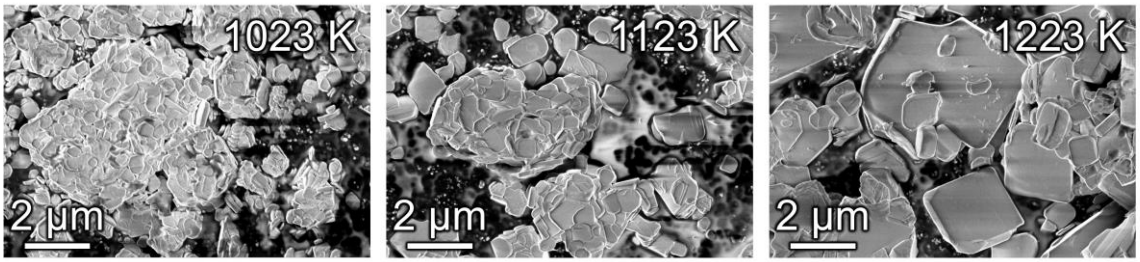

Figure S33. SEM images of $NaGdTiO_{2.2}S_{1.8}$ obtained *via* SSR at 1023–1223 K.

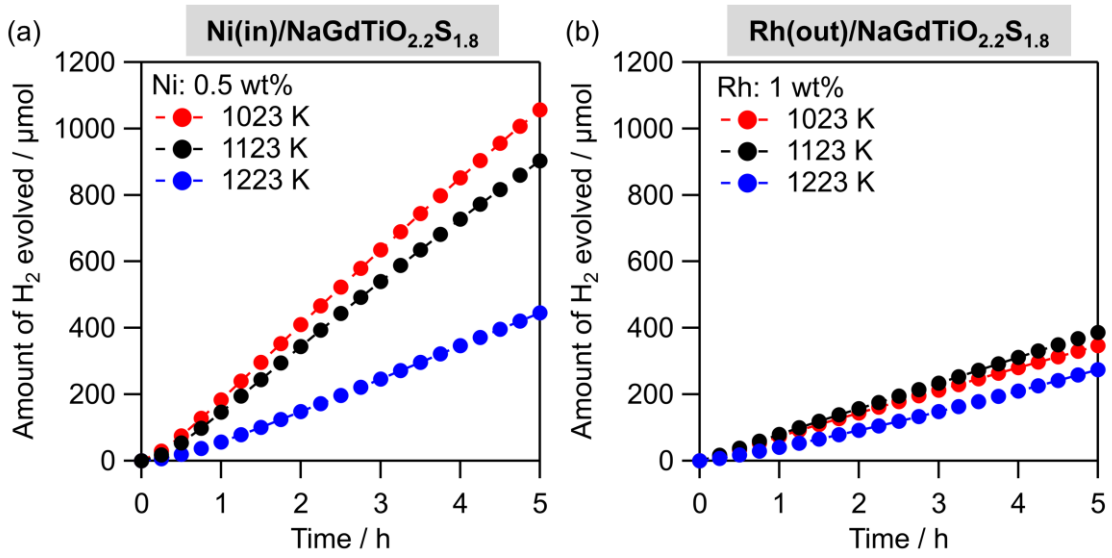

Figure S34. Time courses of photocatalytic H_2 evolution on (a) Ni(in)/$NaGdTiO_{2.2}S_{1.8}$ and (b) Rh(out)/$NaGdTiO_{2.2}S_{1.8}$ synthesized *via* SSR at 1023–1223 K from water with electron donors (S^{2-} and SO_3^{2-}) under visible light ($400 < \lambda < 800$ nm).

References

1 Y. Ishii, H. Suzuki, D. Kato, O. Tomita, A. Nakada and R. Abe, *Chem. Sci.*, 2025, **16**, 16534–16541.
2 I. A. Zvereva, O. I. Silyukov and M. V. Chislov, *Russ. J. Gen. Chem.*, 2011, **81**, 1434.
3 H. B. Mark. Jr., *J. Electroanal. Chem.*, 1964, **8**, 253–261.